Godinho, L.; Redondo, J.; Amado-Mendes, P. (2019). The method of fundamental solutions for the analysis of infinite 3D sonic crystals. Engineering Analysis with Boundary Elements. 98:172-183. https://doi.org/10.1016/j.enganabound.2018.09.015

The Method of Fundamental Solutions for the Analysis of Infinite 3D Sonic Crystals

L. Godinho[1*], J. Redondo [2], P. Amado-Mendes [1]

[1]*ISISE, Dept. Civil Engineering, University of Coimbra, Portugal*

[2] *Instituto de Investigación para la Gestión Integrada de Zonas Costeras, Gandia, Universitat Politècnica de València*

**contact author: lgodinho@dec.uc.pt*

Abstract

The use of periodic structures in acoustic applications has interested the scientific community in the last two decades. Although in-depth research has been thoroughly performed, many issues have still not been solved. The computational analysis of sonic structures using realistic 3D models still poses significant problems, and most of the published results correspond to 2D problems. Indeed, analysing 3D problems of such structures using conventional methods demands large computational resources, which may be prohibitive. The present paper proposes a new approach for such 3D problems making use of a highly efficient Method of Fundamental Solutions (MFS) approach to deal with sonic crystals made of 3D scatterers, which are infinitely repeated with constant spacing along one direction. The proposed method makes use of a special form of the acoustic fundamental solutions which can be highly efficient in such analysis, while allowing just the cell that is repeated to be effectively modelled. Verification of the model is provided by first comparing its results with those from an ACA-MFS model, and then with those resulting from a FDTD algorithm. A parametric study is here presented, with results revealing the true 3D character of the computed responses, and evidencing the formation of acoustic band-gaps at specific frequency bands associated with the Bragg effect.

Keywords: 3D, MFS, sonic crystal, infinite periodic structure

1 Introduction

Acoustic metamaterials and sonic crystals have been a major research topic of the scientific community dealing with acoustics in the last years, mostly since the publication of the pioneering work of Martínez-Sala et al. [1]. Indeed, in that work, the analysis of an artistic sculpture made from a spatially periodic arrangement of cylindrical steel tubes revealed the capacity of such arrangements to filter sound energy at specific frequency bands, forming the so-called acoustic band-gaps. Many other studies then followed, and engineering applications of such concept soon started to be analysed including their use as noise protection devices, such as noise barriers. The works of Sánchez-Pérez et al. [2], Umnova et al. [3] or Martínez-Sala et al. [4] indeed presented some of the works dedicated to such application of sonic crystals, demonstrating their potential in sound attenuation. Later, Castiñeira-Ibáñez et al. [5] presented a study on the manufacturing and characterization of a sonic crystal barrier using a fractal arrangement, showing the good behaviour and feasibility of such solutions.

A challenge of the analysis of sonic crystals is related to their correct and accurate modelling using numerical techniques. Even in the 1990's some proposals started to emerge, including the early works by Kafesaki and Economou [6] in which the Multiple Scattering Theory (MST) is applied to the analysis of a periodic array of elastic spheres embedded in a fluid medium. Plane-wave expansion methods and wavelet-based methods have also been tried in the works of Cao et al. [7] and Yan and Wang [8] for the analysis of sonic crystals. More general numerical methods such as the Finite Difference Time Domain (FDTD) Method [9] or the Boundary Element Method (BEM) [10] were also applied to compute the band structure of different sonic crystal configurations. Koussa et al. [11] also used the BEM to study the effect of complementing a traditional noise barrier

with a sonic crystal. Perhaps one of the most promising developments using the BEM was presented by Karimi et al. [12], implementing what the authors called a Periodic BEM to analyse large arrays of periodically distributed acoustic scatterers. The Finite Element Method (FEM) has also been used, for example, in the definition of an engineering approach for sonic crystal barrier design, using overlapping two-dimensional FEM models [13]; however, the correct incorporation of the 3D character of the generated wavefields in 3D sonic crystals is still not completely demonstrated for this approach.

The more recently developed meshless methods have already been applied in the context of sonic crystals, although available literature is more limited. Two such examples are the works of Zheng et al. [14,15], in which methods based on Radial Basis Functions (RBF) were applied for the analysis of the band structure of in-plane and anti-plane elastic waves in 2D sonic crystals, and of Yan et al. [16], who also used RBF-based techniques to compute the band structure in sonic crystals.

One particular meshless method that has been significantly developed for acoustic analysis is the so-called Method of Fundamental Solutions (MFS) [17,18]. The concept of the MFS is quite simple, taking into consideration that the acoustic wavefield in the presence of scatterers can be reproduced by means of the superposition of the effects of multiple sources, each with an a-priori unknown amplitude. However, the method revealed high potential for acoustic applications, showing good convergence properties and high accuracy even when compared with more conventional methods [19].

The application of the MFS in the field of sonic crystal analysis is due to Martins et al. [20], who proposed its use to evaluate the insertion loss provided by a periodic 2D structure made of rigid scatterers. In that work, the authors addressed the application of the MFS for modelling traffic noise attenuation in a 2D approach, demonstrating that significant computational advantages are obtained when comparing to BEM and FEM

approaches. Later, the work by Santos et al. [21] extended the formulation to allow considering elastic shell scatterers. However, in both works, the classic formulation of the MFS was used, involving the complete formation of the system matrix and thus exhibiting some limitations regarding the maximum problem size that could be addressed. Indeed, it should be noted that the mathematical structure of the MFS leads, in these cases, to the generation of a very large matrix, which is fully populated and demands significant memory requirements. In an attempt to define a more powerful strategy to allow structures with a large number of scatterers (and nodes) to be analyzed, Godinho et al. [22] proposed a 2.5D MFS formulation together with the Adaptive-Cross-Approximation (ACA) technique. In [23], Godinho et al. proposed a new periodic MFS formulation, also using the ACA, to address the case of large periodic finite arrays of scatterers in 3D. The method was found to be very efficient and to allow modelling very large structures while allowing large savings of computational resources.

An important limitation of the above mentioned approaches using the BEM or the MFS is that they pose difficulties when a very large structure, which approaches the behaviour of a sonic crystal of infinite extent, needs to be modelled. Although this can be done using a FEM or FD approach, using periodic boundary conditions, standard BEM and MFS formulations cannot deal with such configurations directly. The present paper proposes a new approach for such 3D problems making use of a highly efficient MFS implementation to deal with sonic crystals made of 3D scatterers, which are infinitely repeated with constant spacing along one direction. For that purpose, a special form of the acoustic fundamental solution for acoustic problems is proposed, which can be highly efficient in such analysis. Indeed, by using such periodic fundamental solution only a very small portion of the structure needs to be modelled, corresponding to the unitary cell that is infinitely repeated along one direction. Using such strategy, very large computational

savings can be obtained, and a very competitive engineering model is defined, surpassing, for example, the limitations of using two overlapping 2D models of [13], or the need to discretize the whole structure and calculate a very large matrix of [23].

In the remaining part of this paper, first, the mathematical formulation of the 3D MFS is presented, together with the standard fundamental solutions for infinite and semi-infinite acoustic media. Then, the proposed periodic fundamental solutions are presented, and a study and discussion on their convergence properties is provided. Verification of the model is then performed by first comparing its results with those from the ACA-PMFS model of [23], in terms of acoustic pressure results, and then with those resulting from a completely independent 3D FDTD algorithm, in terms of insertion loss results. A parametric study is finally presented, with a set of results that reveal the true 3D character of the computed responses and evidence the formation of acoustic band-gaps at specific frequency bands associated with the Bragg effect.

2 Method of Fundamental Solutions for 3D acoustic problems

The propagation of sound within a three-dimensional space can be mathematically given in the frequency domain by the Helmholtz partial differential equation,

$$\nabla^2 p(\mathbf{x}) + k^2 p(\mathbf{x}) = -\sum_{k=1}^{NS} Q_k \delta(\mathbf{x}_k^f, \mathbf{x}), \tag{1}$$

where $\nabla^2 = \frac{\partial^2}{\partial x^2} + \frac{\partial^2}{\partial y^2} + \frac{\partial^2}{\partial z^2}$; p is the acoustic pressure; $k = \omega / c$; $\omega = 2\pi f$; f is the frequency; c is the sound propagation velocity within the acoustic medium; *NS* is the number of sources in the domain; Q_k is the magnitude of the existing sources $\mathbf{x}_k^f$ located at (x_k^f, y_k^f, z_k^f); $\mathbf{x}$ is a field point located at (x, y, z); and $\delta(\mathbf{x}_k^f, \mathbf{x})$ is the Dirac delta generalized function.

The boundary conditions for the problem (for $\mathbf{x}$ in the boundary) are given by:

$$v_n(\mathbf{x}) = \frac{\mathrm{i}}{\omega\rho}\frac{\partial p}{\partial \mathrm{n}}(\mathbf{x}) = \overline{v}_n\ (\mathbf{x}) \qquad \text{in interfaces } S_\upsilon \tag{2a}$$

$$p(\mathbf{x}) = \overline{Z}(\mathbf{x})v_n(\mathbf{x}) \qquad \text{in interfaces } S_Z \tag{2b}$$

where $\overline{v}_n\ (\mathbf{x})$ is the normal particle velocity and $\overline{Z}(\mathbf{x})$ is the surface impedance of a possible absorbing material, which are assumed to be known quantities. Equation (2a) stands for Neumann condition and equation (2b) stands for Robin or impedance boundary condition.

Considering that a source point is placed within this propagation domain, at $\mathbf{x}_0\ (x_0, y_0, z_0)$, it is possible to establish the fundamental solution for the incident sound pressure at a point $\mathbf{x}$, which can be written as

$$G(\mathbf{x}_0, \mathbf{x}) = \frac{\mathrm{e}^{-\mathrm{i}kr}}{4\pi r}, \text{ with } \quad r = \sqrt{(x-x_0)^2 + (y-y_0)^2 + (z-z_0)^2}\ . \tag{3}$$

In the context of noise barrier analysis, it is usually necessary to consider the effect of the ground plane, which generates an additional reflection that interferes with the expected acoustic results. The presence of a perfectly reflecting plane surface, simulating a rigid ground, can be taken into account by using the well-known image-source method. In this technique, the effect of a source point in the presence of a given plane surface can be simulated by considering an additional virtual source, positioned in a symmetrical position with respect to the reflecting plane. Thus, if such plane is defined by $z = 0$, the corresponding Green's function can be written as

$$G_h(\mathbf{x}_0, \mathbf{x}) = \frac{\mathrm{e}^{-\mathrm{i}kr}}{4\pi r} + \frac{\mathrm{e}^{-\mathrm{i}kr_1}}{4\pi r_1}, \text{ with } r_1 = \sqrt{(x-x_0)^2 + (y-y_0)^2 + (z+z_0)^2}\ . \tag{4}$$

The Method of Fundamental Solutions is here used to compute the frequency domain response in a three dimensional halfspace surrounding a set of acoustic scatterers. This

solution is computed as a linear combination of fundamental solutions for a set of NVS virtual sources, with amplitude A_l (with $l = 1,...,NVS$). These sources are placed outside the domain of interest (inside the scatterers), to avoid singularities. Thus, the pressure field around the scattering objects can be computed as:

$$p(\mathbf{x}) = \sum_{l=1}^{NVS} A_l G_h\left(\mathbf{x}_l^v, \mathbf{x}\right) + P_{inc}(\mathbf{x}), \tag{5}$$

where the coefficients A_l are unknown amplitudes which are computed by imposing the appropriate boundary conditions at a set of NCP points (collocation points) placed along the surfaces $S = S_v \cup S_Z$ and $G_h\left(\mathbf{x}_l^v, \mathbf{x}\right)$ is the fundamental solution at point $\mathbf{x}$ for a virtual source placed at $\mathbf{x}_l^v$. $P_{inc}(\mathbf{x})$ represents a generic incident wavefield, generated by any source within the acoustic domain. In the MFS model here developed, the Green's function presented in Equation (4) is used. In this work, an equal number of collocation points and virtual sources is assumed, which allows obtaining a $NVS \times NVS$ system. This system is built by prescribing at each collocation point $\mathbf{x}_m$, placed in the boundaries of the scatterers, the conditions defined in equations (2). By applying this procedure one obtains:

$$\sum_{l=1}^{NVS} A_l \frac{\partial G_h\left(\mathbf{x}_l^v, \mathbf{x}_m\right)}{\partial n} = -\frac{\partial P_{inc}(\mathbf{x}_m)}{\partial n}, \tag{6}$$

$$\sum_{l=1}^{NVS} A_l G_h\left(\mathbf{x}_l^v, \mathbf{x}_m\right) + P_{inc}(\mathbf{x}_m) = \\ = \frac{\mathrm{i}\overline{Z}(\mathbf{x}_m)}{\rho\omega}\left(\sum_{l=1}^{NVS} \mathrm{A}_l \frac{\partial G_h(\mathbf{x}_l^v, \mathbf{x}_m)}{\partial n} + \frac{\partial P_{inc}(\mathbf{x}_m)}{\partial n}\right). \tag{7}$$

Equation (6) is applied for the case of rigid surfaces, while equation (7) is employed if it is required to assign absorption to the surfaces of the model. For both cases, a resulting

$NVS \times NVS$ system is obtained, which after being solved makes it possible to obtain the acoustic pressure at any point of the domain by applying equation (5).

3 Method of Fundamental Solutions for an infinite periodic system

In the context of the present paper, the interest is focused in the analysis of the scattering by infinite sets of objects, placed above a horizontal plane, and arranged periodically along one direction (see Figure 1). For that scenario, using the fundamental solution described in equation (4) leads to the requirement of modelling each of the scatterers using the MFS, distributing collocation points and virtual sources associated to each scatterer. To accurately simulate an infinite array, it would become necessary to consider a large number of scatterers, in order to avoid diffraction effects that should not occur for an infinite array.

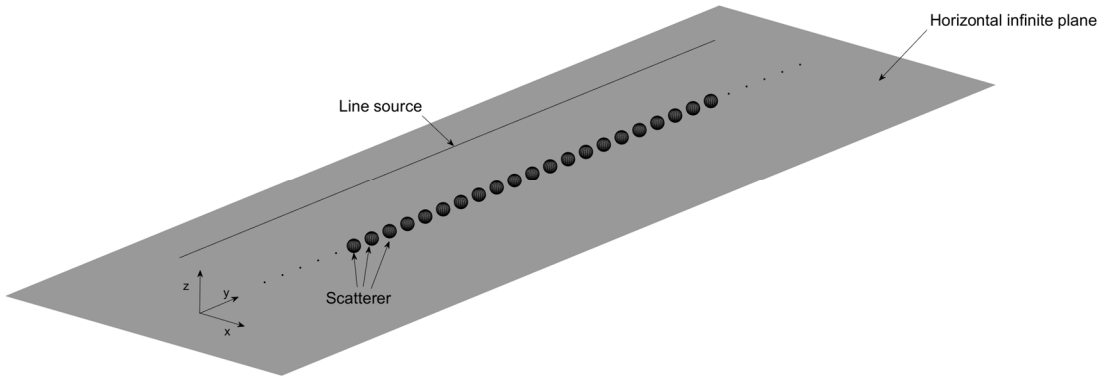

Figure 1 – Schematic representation of a regular array of scatterers, periodically spaced along one direction and illuminated by a line source.

The simplest form to analyse this problem is to bear in mind that, for a problem with a periodic array of scatterers and a periodic source (as for example the line source illustrated in Figure 1) aligned with the axis of periodicity, the acoustic field must also exhibit periodicity. If a periodicity a is assumed, this means that

$$p(\mathbf{x}_{n\times a}) = p(\mathbf{x}) \text{ , with } \mathbf{x} = (x, y, z) \text{ and } \mathbf{x}_{n\times a} = (x, y + n\times a, z) \tag{8}$$

It can also be stated that, in the context of a purely periodic system, the position of each virtual source *l* inside scatterer *i* (with *i* being an integer ranging from $-\infty$ to $+\infty$), can be written as

$$\mathbf{x}_{l,i}^{v} = (x_l^v, y_l^v + i\times a, z_l^v) \tag{9}$$

Given this previous assumptions, if a set of NVS*i* virtual sources and collocation points is used for each scatterer *i*, and the amplitudes of each virtual source located at $\mathbf{x}_{l,i}^{v}$, are given by $A_{l,i}$, then

$$A_{l,-\infty} = \cdots = A_{l,-1} = A_{l,0} = A_{l,1} = \cdots = A_{l,+\infty} = A_l \,. \tag{10}$$

So, the pressure field at any point $\mathbf{x}$ of the propagation domain may also be written as (designating by $P_{inc}^{per}(\mathbf{x})$ the incident field coming directly from a possible source, which must also have the same periodicity with that of the system):

$$p(\mathbf{x}) = \sum_{l=1}^{NVSi}\left(A_l \sum_{i=-\infty}^{+\infty} G_h\left(\mathbf{x}_{l,i}^{v}, \mathbf{x}\right)\right) + P_{inc}^{per}(\mathbf{x}) \,. \tag{11}$$

Observing equation (11), it can be inferred that the analysis of an infinite periodic structure, with periodicity *a* along the direction *y* can be performed using the MFS by considering an adapted fundamental solution, obtained by also considering the fundamental solution to have the same periodicity as the physical system. Thus, a possible fundamental solution for this case can be written as

$$G_{h,per}\left(\mathbf{x}_l^v, \mathbf{x}\right) = \sum_{i=-\infty}^{+\infty} G_h\left(\mathbf{x}_{l,i}^{v}, \mathbf{x}\right) \text{ with } \mathbf{x}_{l,i}^{v} = (x_l^v, y_l^v + i\times a, z_l^v) \tag{12}$$

Although this simple equation can indeed be used as the basis of a periodic MFS formulation, it should be noted that the involved summation can pose convergence

problems, and require a very large number of terms to converge, thus leading to very long computational times. However, at this point it should be noted that equation (12) just represents an infinite summation of periodically placed sources along one direction. It is important to recall that a 3D acoustic source (equation 3) can, following a spatial Fourier transformation, be represented as a summation of 2D sources with varying axial wavenumbers (as described in detail in Tadeu and Godinho [24] or in Godinho et al. [25]), such that

$$G(\mathbf{x}_0,\mathbf{x})=\frac{\mathrm{e}^{-ikr}}{4\pi r}=-\frac{\mathrm{i}}{8\pi}\int_{-\infty}^{+\infty}\mathrm{H}_0^{(2)}(k'r')\mathrm{e}^{-\mathrm{i}k_y(y-y_0)}\mathrm{d}k_y\,, \tag{13}$$

where $k'=\sqrt{\left(\frac{\omega}{c}\right)^2-k_y^2}$ (with $\mathrm{imag}(k')<0$), and $r'=\sqrt{(x-x_0)^2+(z-z_0)^2}$. Discretizing this integral in regular intervals of dk_y, one obtains the acoustic field in the form of an infinite summation as

$$G(\mathbf{x}_0,\mathbf{x})=-\frac{\mathrm{i}}{8\pi}\sum_{n=-\infty}^{+\infty}\mathrm{H}_0^{(2)}(k'r')\mathrm{e}^{-\mathrm{i}\times dk_y\times n\times(y-y_0)}\times dk_y\,. \tag{14}$$

The introduction of such a discretization is, following the same references [24, 25], equivalent to considering a set of point sources equally spaced of L along the axis of periodicity, such that $dk_y=\frac{2\pi}{L}$. So, if L=a, it can be stated that

$$-\frac{\mathrm{i}}{8\pi}\sum_{n=-\infty}^{+\infty}\mathrm{H}_0^{(2)}(k'r')\mathrm{e}^{-\mathrm{i}\times\frac{2\pi}{L}\times n\times(y-y_0)}\times\frac{2\pi}{L}=\sum_{i=-\infty}^{+\infty}G\left(\mathbf{x}_{l,i}^{v},\mathbf{x}\right). \tag{15}$$

Following these considerations, and now assuming that an additional image source is considered to simulate a horizontal plane, the periodic fundamental solution for a halfspace can be written as

$$G_{h,per}\left(\mathbf{x}_l^v,\mathbf{x}\right)=\sum_{i=-\infty}^{+\infty}G_h\left(\mathbf{x}_{l,i}^v,\mathbf{x}\right)=-\frac{\mathrm{i}}{4a}\left(\sum_{n=-\infty}^{+\infty}\left(\mathrm{H}_0^{(2)}(k'r')+\mathrm{H}_0^{(2)}(k'r'')\right)\mathrm{e}^{-\mathrm{i}\times\frac{2\pi}{a}\times n\times(y-y_0)}\right) \qquad (16)$$

where $r''=\sqrt{(x-x_0)^2+(z+z_0)^2}$. This summation is known to have good convergence properties [24,25] and can be a more efficient alternative to equation (12).

To test the convergence of both presented alternatives (equations 12 and 16), a compact convergence study is next presented. For that purpose, let us consider a halfspace domain in which a point load is located, at $\mathbf{x}_0=\left(0.0;\ 0.0;\ 0.5\right)$, and that the response is to be computed at a receiver point located at $\mathbf{x}=\left(0.1;\ 0.25;\ 0.5\right)$; a periodicity of 0.5m is considered and a sound propagation velocity of 343 m/s is assumed. Figure 2 depicts the convergence of equations (12) and (16) when the harmonic source oscillates with a frequency of 500 Hz. In the presented plots, it can be seen that the computations performed with equation (12) (Figure 2a1) converge slowly to the solution, oscillating around the correct value as more terms (sources) are added to the summation. Indeed, observing this plot and also that of Figure 2b1, which depicts the convergence in terms of relative error as a function of the number of terms, it can be seen that even for 1000 terms a relative error of 10^{-4} has not yet been reached. By contrast, observing the plots of Figures 2a2 and 2b2, it can immediately be realized that, with just 5 terms, this level has already been reached, revealing a much faster convergence and thus an increased computational efficiency. In Figure 3 similar results are plotted for a frequency of 2000 Hz, and for that case the difference between the convergence of the two solutions is even more evident. However, it should be stressed that both approaches are converging to the same solution, as can be seen in Figures 2a and 3a. To complement this analysis, Figure 4 presents the convergence curve for two additional domain points, for 2000 Hz, confirming the same fast convergence rate observed before.

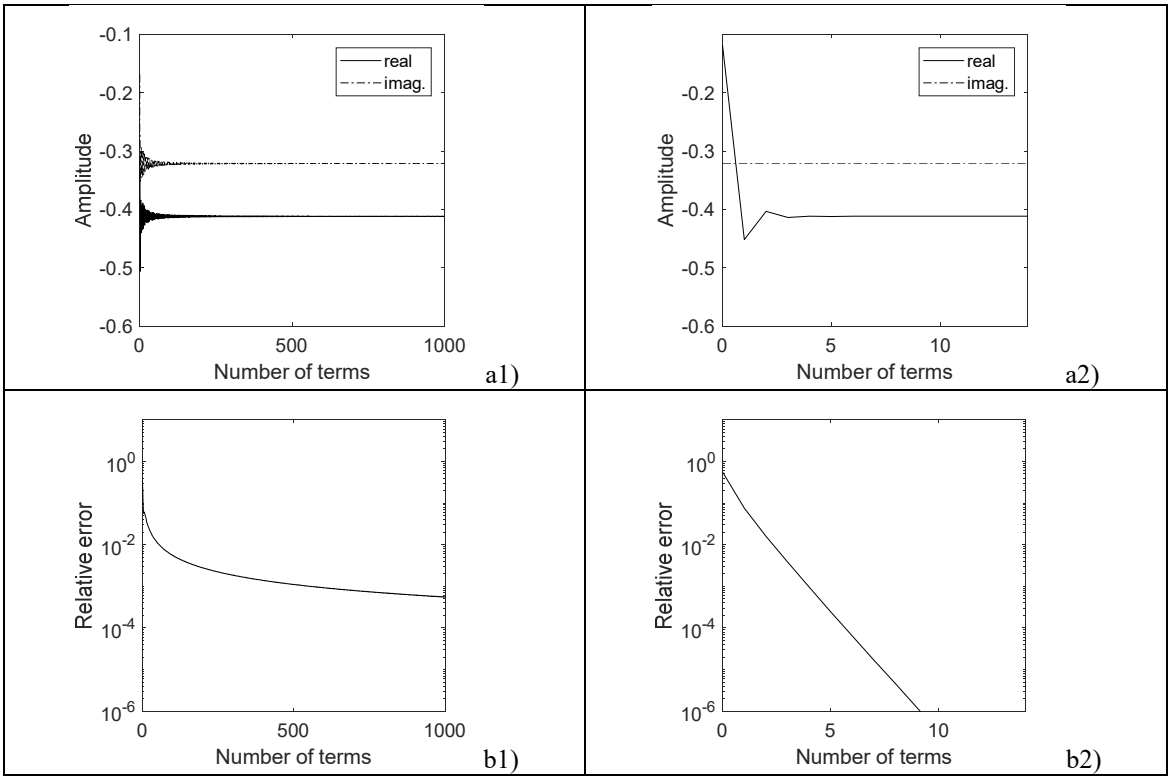

Figure 2 – Convergence of the two periodic fundamental solutions for a frequency of 500 Hz. In a1 and a2 the calculated real and imaginary parts of the response are depicted, and in b1 and b2 the relative error is shown. a1 and b1 correspond to solutions computed using equation (12), and a2 and b2 to solutions computed with equation (16).

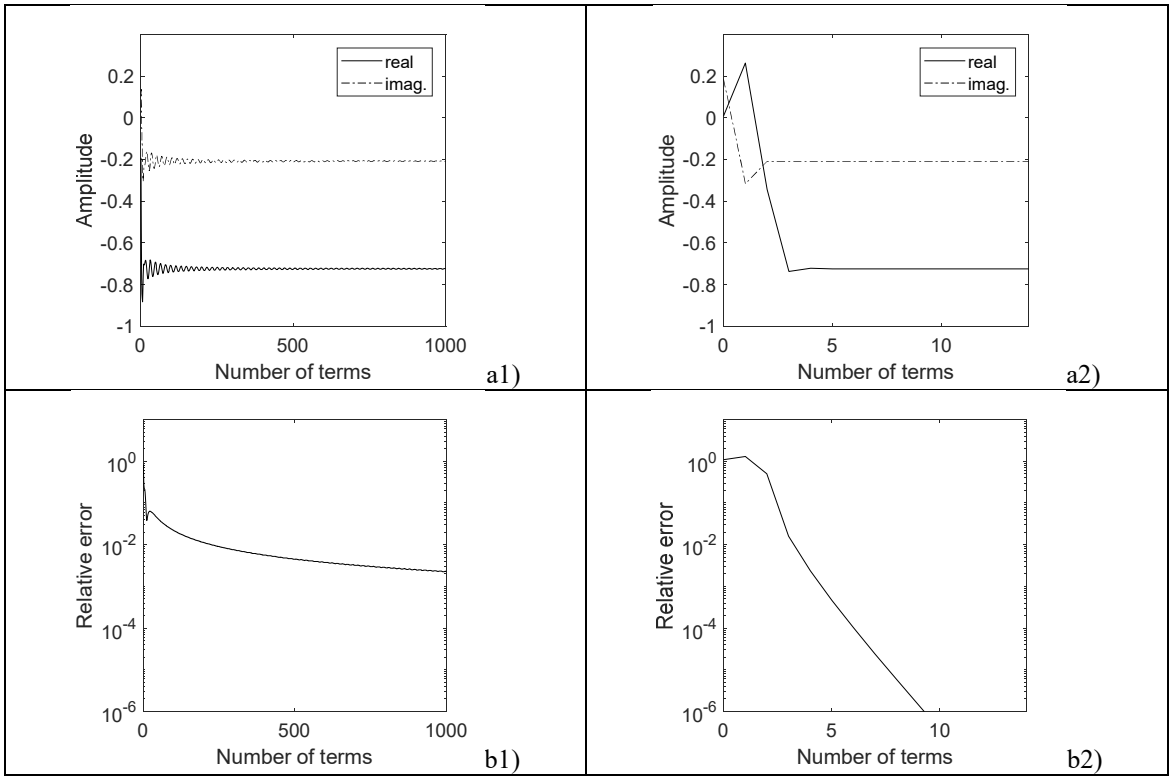

Figure 3 – Convergence of the two periodic fundamental solutions for a frequency of 2000 Hz. In a1 and a2 the calculated real and imaginary parts of the response are depicted, and in b1 and b2 the relative error

is shown. a1 and b1 correspond to solutions computed using equation (12), and a2 and b2 to solutions computed with equation (16).

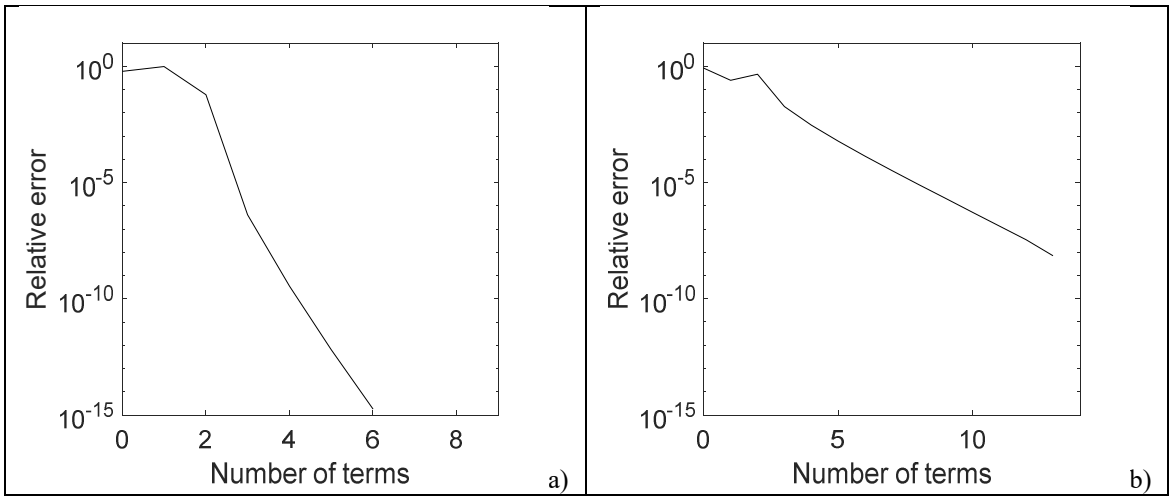

Figure 4 – Convergence of the periodic fundamental solution of equation (16), for a frequency of 2000 Hz, considering two different domain points: a) $\mathbf{x} = (0.1;\ 0.0;\ 0.1)$; b) $\mathbf{x} = (0.1;\ 0.0;\ 0.5)$.

Although very good convergence has been observed in all previous analysis, it is important to note that a particular case occurs when the source and the receiver points coincide in the x-z plane. For that case, equation (16) cannot be calculated, as the involved Hankel function tends to infinite. Although in the context of the proposed MFS application this issue can easily be avoided by always using slightly different x and z coordinates for the virtual sources and for the collocation points, it is important to assess the behaviour of the proposed fundamental solution in the vicinity of the source point. Figure 5 illustrates the corresponding responses for 2000 Hz, when the receiver points are $\mathbf{x} = (0.0;\ 0.01;\ 0.5001)$ (Figures 5a1 and 5a2) and $\mathbf{x} = (0.0;\ 0.1;\ 0.5001)$ (Figures 5b1 and 5b2). For the illustrated case, the source and the receiver points are almost coincident in the x-z plane, with a distance between them of just 0.0001 m in that plane, and distances of 0.01 m and 0.1 m are considered along the y axis (axis of periodicity). The evolution of the real and imaginary parts of the response with increasing numbers of terms clearly reveals that the required number of terms is very high, and convergence is only attained when 5000 or more terms are considered. It should be noted that, for this case, due to the close proximity between source and receiver, the importance of evanescent waves (which

are the only ones to propagate when $|k_y| > \omega/c$) is much higher, and so the number of terms necessary for convergence considerably increases. However, convergence can still be reached, although after a marked oscillatory behavior that occurs at the beginning of the process. These results indicate that the proposed fundamental solution of equation (16) can be used even for the case of the receiver being very close to the source, although longer convergence times are expected.

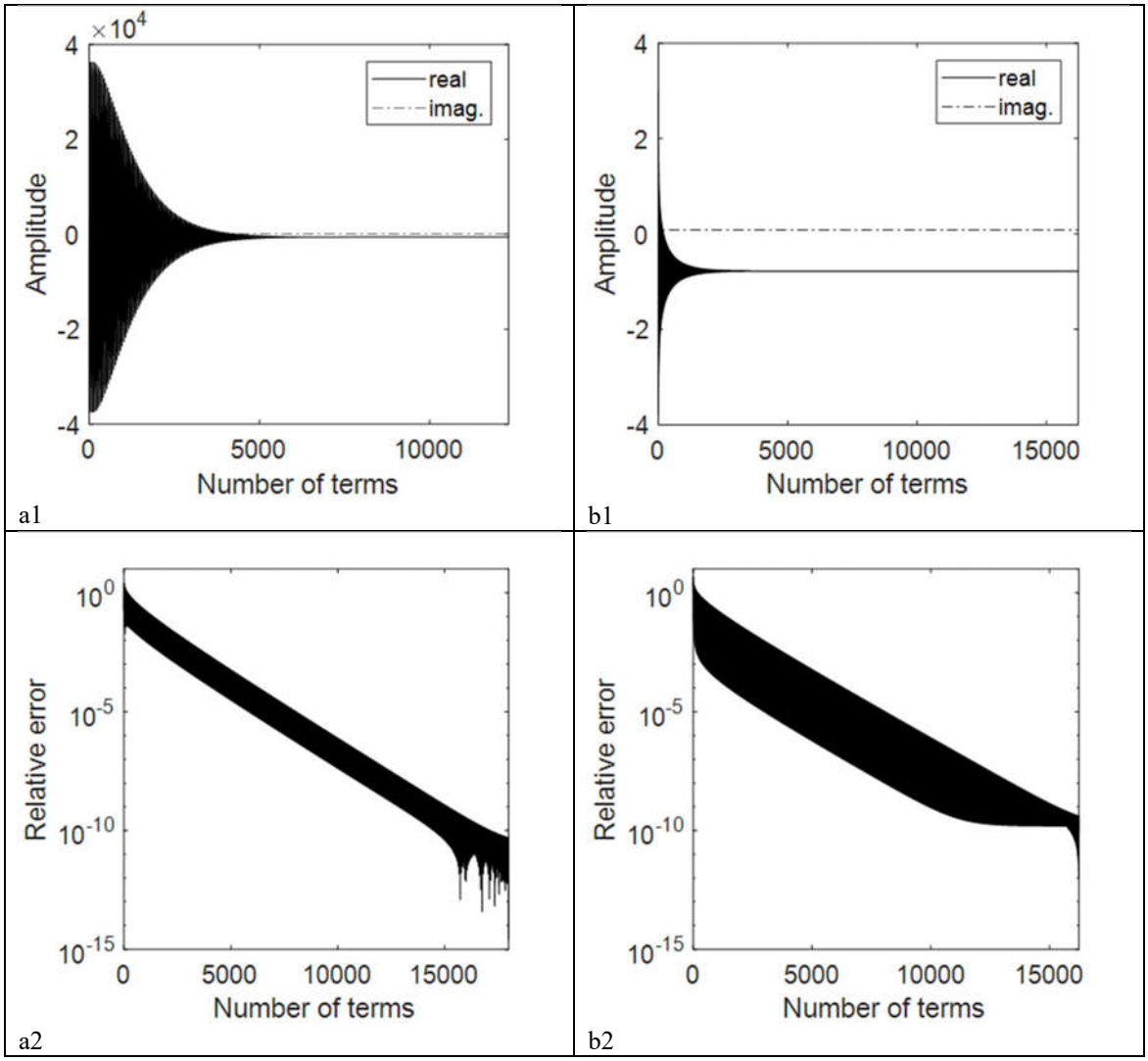

Figure 5 – Convergence of the periodic fundamental solution of equation (16), for a frequency of 2000 Hz, considering two domain points very close to the source in the x-z plane: a) $\mathbf{x} = (0.0;\ 0.01;\ 0.5001)$; b) $\mathbf{x} = (0.0;\ 0.1;\ 0.5001)$.

To have a better view of the number of terms required for convergence as a function of receiver position, Figure 6 depicts the required number of terms for each point over a x-

z plane positioned at y=0.01m and y=0.1m, for a frequency of 2000 Hz. These two plots clearly corroborate the findings described before, and evidence the presence of a marked peak occurring when the source and receiver are very close to each other. In the most part of the domain, less than 10 terms are required, and even at intermediate regions no more than 30 terms are needed to attain convergence. Results computed for other frequencies (not shown) also evidence the same behaviour.

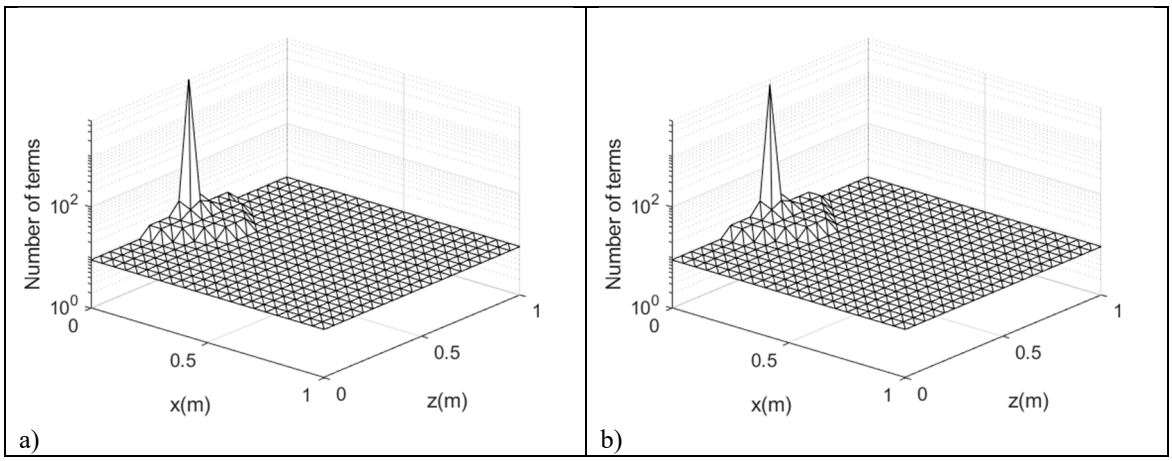

Figure 6 – Number of terms required for convergence by equation (16), for a frequency of 2000 Hz, considering different points in the x-z plane: a) y=0.01m; b) y=0.1m. A relative error of 10^{-5} was considered for convergence.

4 Verification of the proposed algorithm

In order to verify the proposed MFS model, its results must be compared with those provided by alternative numerical strategies. For that purpose, the model proposed by the authors in [23] is used as a reference, and a test scenario is defined to perform the required comparisons. In this scenario, the individual scatterer assumes the simple shape of a sphere (Figure 7a), with radius of 0.1 m, and it is disposed along the y axis with a periodicity of 0.3 m, over a rigid horizontal plane (halfspace). The scatterers are centred at x=0.6 m and z=0.6 m, and are illuminated by a line load positioned at x=1.2 m and z=0.3 m. The response is computed over a line of receivers positioned between x=-1.0 m and x=-6.0 m, at y=0.0 m and z=0.3 m, as depicted in Figure 7b.

To illustrate the global behaviour, an excitation frequency of 3000 Hz is chosen, and the results are calculated using the proposed model (which in fact simulates the infinite character of the periodic array) and the model of [23], with different numbers of scatterers. Sets of 17, 33, 41 and 81 scatterers are tested and the results presented in Figure 8, in terms of absolute acoustic pressure. As can be seen in that figure, the results calculated with a reduced number of scatterers follow the response provided by the proposed model in a very rough manner, and the detail of the oscillatory character of the response is missed, particularly for receivers placed further away from the source. As the number of modelled scatterers is increased, the calculated response becomes progressively closer to that of the proposed model, and for the higher number of scatterers (81) the two responses finally become very close. However, even for that case, small differences can be identified, as depicted in Figure 8b.

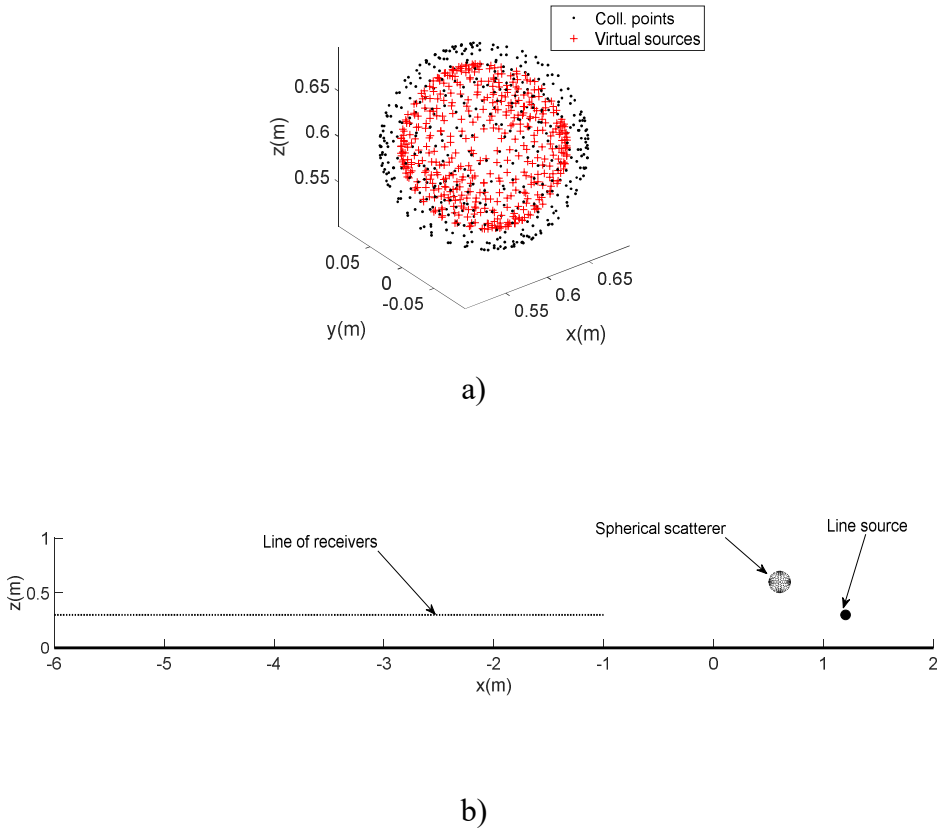

Figure 7 – Schematic representation of the test problem: a) spherical scatterer with radius 0.1m, and 456 collocation points; b) 2D view of the test scenario along the x-z plane for y=0.

Globally, the results presented here indicate that the proposed model is correctly predicting the acoustic pressure behind the periodic structure, and that the MFS model which only considers a finite number of scatterers progressively approaches that response as the number of scatterers increases. Moreover, it should be stated that a very significant CPU time difference between the two methods is registered in this calculation, with only a fraction of the time being required by the proposed model. Considering, for example, the case with 81 scatterers, the CPU time required by the model proposed here is about 20% of the time required by the already efficient periodic ACA MFS model proposed in [23] for finite periodic structures.

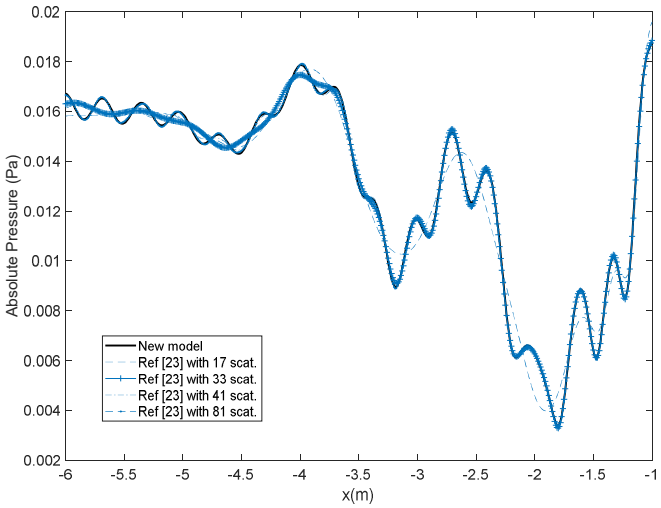

a)

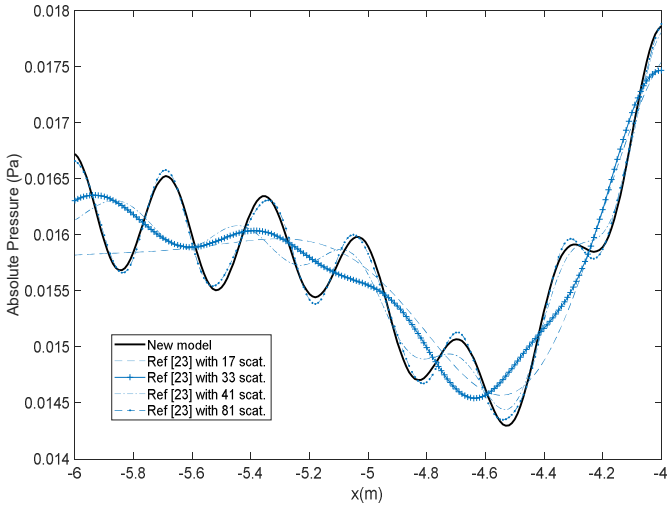

b)

Figure 8 – a) Comparison of the proposed model results with those computed using Ref. [23], for different numbers of scatterers; b) zoomed view of the comparison.

5 Numerical experiments

The model proposed and described in the previous sections has been used to perform a number of numerical simulations, in order to better understand the behaviour of sonic crystals, correctly incorporating their 3D character. For that purpose, a generic configuration has been defined, as schematically illustrated in Figure 9, considering a lattice constant *a* and assuming that the scatterers have a circular cross section of diameter *D*. The acoustic system is illuminated either by a plane wave, propagating from the left side of the structure. For the purpose of insertion loss (IL) calculations, a grid of 11×6×3 receivers is used, as depicted in the figures.

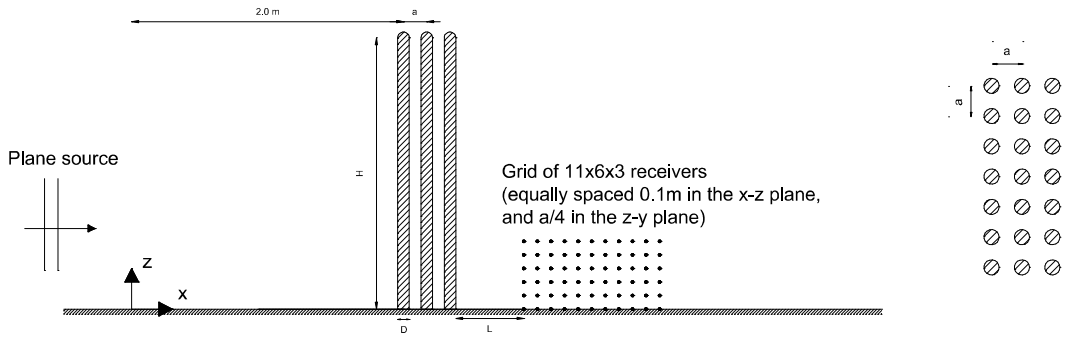

a) b)

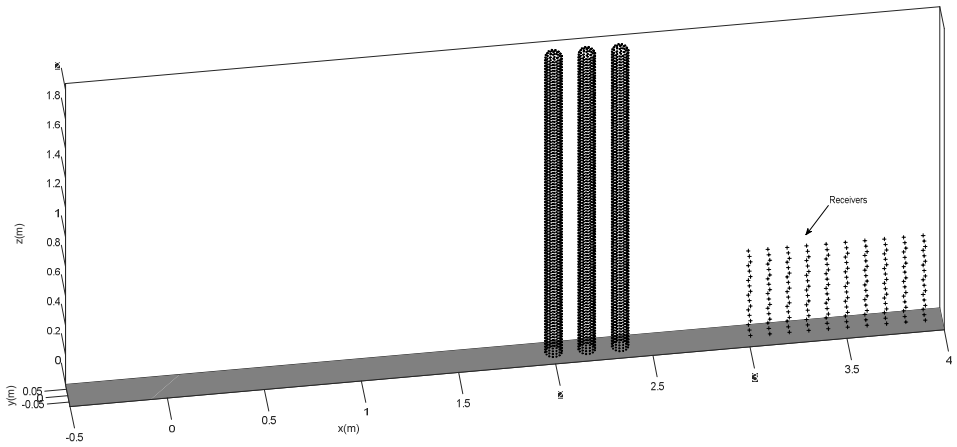

c)

Figure 9 – Side (a) and top (b) views of the sonic crystal used in the numerical applications. In (c) a 3D view of an example problem is shown, considering scatterers with a height of 2.0m, periodically repeated along the y direction.

In a first set of results, let us analyse the insertion loss provided by a sonic crystal structure defined considering a height of 2.0 m and a lattice constant (periodicity) of 0.1715 m; this value is defined so that the theoretical band-gap, generated by the Bragg effect, occurs at f=343/2/a=1000 Hz. A plane wave is assumed to illuminate the system, and the insertion loss is calculated as the difference between the sound pressure levels (averaged at the receivers' grid observed in Figure 9a) computed without and with the structure:

$$IL = L_{without} - L_{with}\ [dB] \tag{17}$$

For the purpose of IL calculations, the grid of receivers is positioned 0.5 m behind the scatterers (L=0.5 m in Figure 9a).

Figure 10 illustrates the insertion loss curves calculated in 1/3 octave bands between 100 Hz and 3150 Hz, considering 3 rows of scatterers and different radii for the scatterers. These radii are defined as being 50% (Figure 10a), 75% (Figure 10b) or 90% (Figure 10c) of the maximum possible radius in a square lattice (*a/2*). To allow a cross-verification

with a completely independent method, in the same figure the IL curves calculated using a Finite-Difference-Time-Domain (FDTD) algorithm are also presented. Further details of the algorithm used can be found at [26]. In that calculation, a spatial step of 0.5 cm was used, equivalent to at least 12 points per wavelength, together with a staggered grid with about 14×10^6 points. Comparing the results calculated using both methods, it is clear that they both identify the same type of behaviour for the three cases, with IL peaks occurring at specific frequencies of 1000 Hz and 2500 Hz. The amplitudes of the IL predicted at these frequencies are very similar, and significant discrepancies are only visible for the larger sized scatterers (with a radius of 75% and 90% of the maximum) for which the proposed MFS predicts an IL around 1.5 dB higher than the FDTD method at the first IL peak. At lower frequencies, it is clear that the results are not perfectly coincident, and that visible divergences can be identified in particular for the larger scatterers (radius of 90% of the maximum). However, in general, it can be said that similar qualitative and quantitative predictions are made in terms of IL by these two methods.

From a physical point of view, a first band-gap emerges around 1000 Hz for all configurations, with considerable IL being registered, occurring at the frequency theoretically estimated considering the Bragg effect. As larger scatterers are considered, the insertion loss tends to increase, and particularly for a radius of 90% of the maximum this band-gap becomes broader, covering a wider frequency range. A second band-gap also occurs at higher frequencies, which however seems to be somewhat dependent on the diameter of the scatterers.

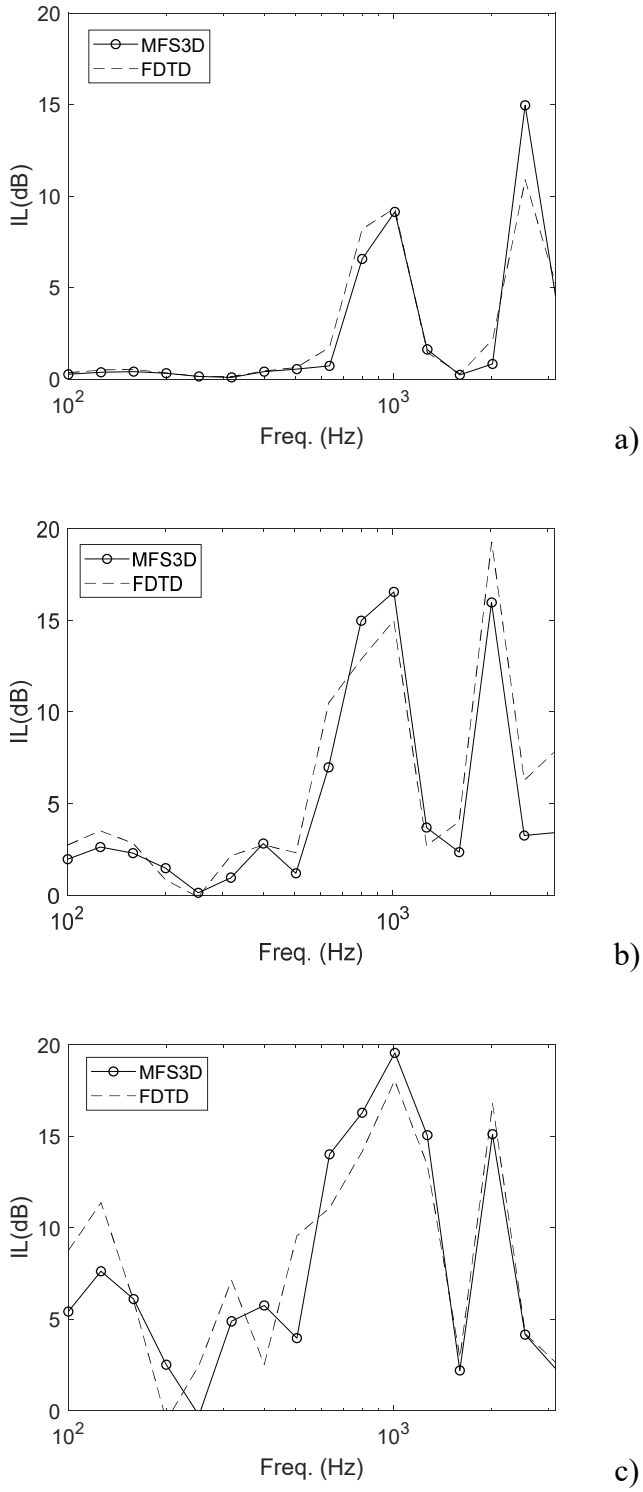

Figure 10 – Insertion loss in 1/3 octave bands computed with FDTD and MFS for sonic crystals 2m high and 3 rows, considering different radii for the scatterers. These radii are defined as a percentage of the maximum allowed radius for the defined square lattice (with a value of 0.08575 m, half of the lattice parameter): a) 50%; b) 75%; c) 90%.

Figure 11 illustrates the insertion loss curves calculated considering 2, 3 or 4 rows of scatterers. The presented results clearly reveal that below 600 Hz the insertion loss is

essentially negligible, and the structure provides almost no protection to the receivers positioned behind it. As before, a first band-gap is visible for all cases at 1000 Hz, matching the theoretically estimation for the Bragg effect and reaching almost 15 dB for the structure with 4 rows. In this plot, it is clear that as more rows are considered, higher IL values are reached. In all curves, a second band-gap is also clearly visible, occurring at the same frequency (of around 2500 Hz) for the three cases.

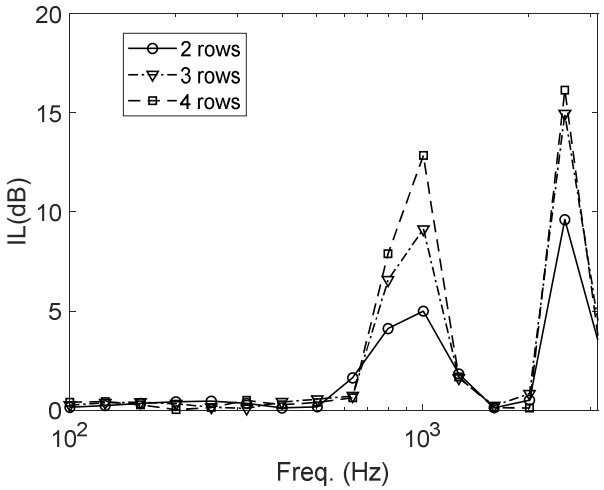

Figure 11 – Insertion loss in 1/3 octave bands computed for sonic crystals 2m high, and with 2, 3 and 4 rows of scatterers.

To better understand the sound pressure level (SPL) distribution that occurs in the different zones of the IL curve, Figure 12 exhibits SPL maps calculated for frequencies of 500 Hz, 1000 Hz, 1600 Hz and 2500 Hz, considering 3 rows of scatterers. Observing the presented plots, it is clear that the effect of the barrier is almost null for 500 Hz and 1600 Hz, and the energy passes through the obstacle with very little attenuation. By contrast, in the band-gap frequencies of 1000 Hz and 2500 Hz, a shadow zone is clearly visible at receivers behind the sonic crystal, and particularly at lower heights. It should be noted that, for receivers placed further away from the ground, the sound energy is not influenced by the barrier, and just passes above it; at lower heights, the energy reaching the receivers is a combination of two different paths: one corresponding to the energy

passing through the barrier, and the other to the energy diffracted by the top of the scatterers. Observing the results for 1000 Hz, the effect of the interaction with the ground is also noticeable, with the energy being reflected at that rigid surface back to the propagation medium. Another interesting feature is that the attenuation effect occurring behind the sonic crystal seems to be extended to quite large distances from the structure, and is still very noticeable 4 m behind it. This feature is particularly evident in Figure 12d, for the higher frequency, for which the barrier protection seems to occur almost for the full grid behind the barrier and at heights lower than 2 m. That behavior seems to indicate a weaker diffraction effect than that seen on conventional (wall-type) barriers.

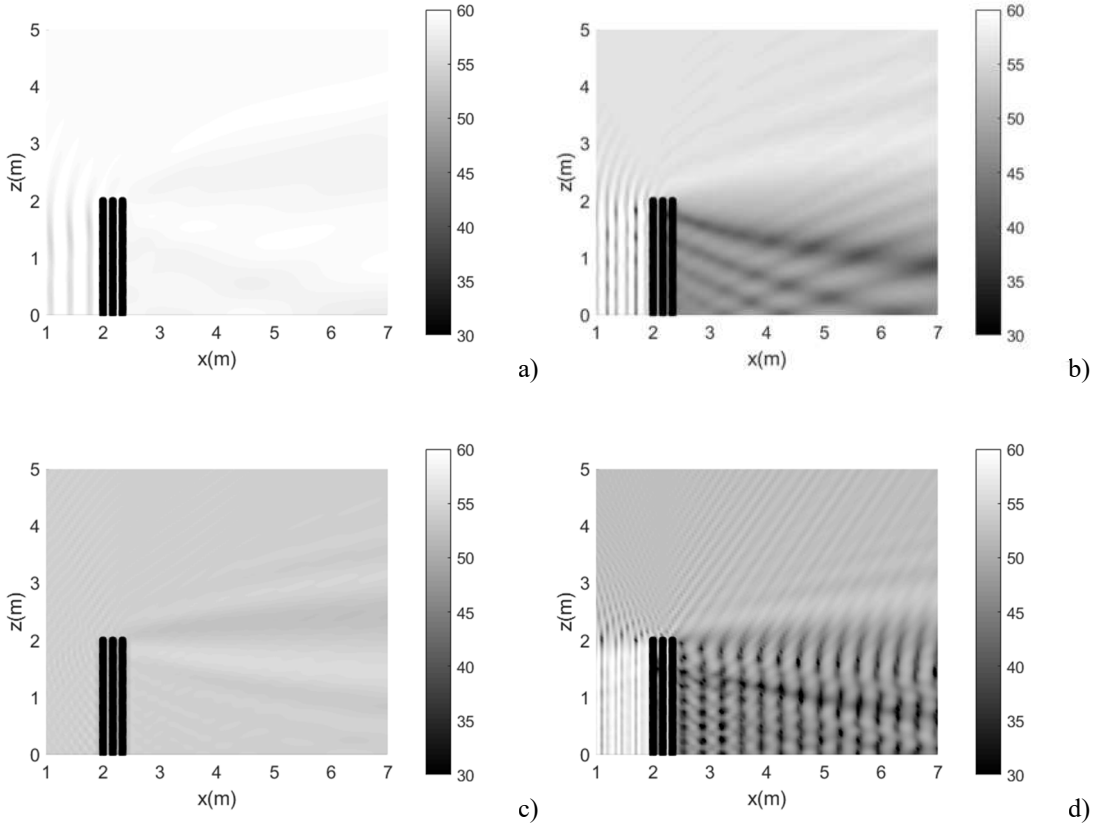

Figure 12 – SPL maps for sonic crystals 2m high, with 3 rows of scatterers, for a x-z plane located at y=a/2 and for: a) 500 Hz; b) 1000 Hz; c) 1600 Hz; d) 2500 Hz.

Indeed, one point to be addressed in this study is related to the importance of considering the 3D effect of the sonic crystal. In most of the published studies, a 2D approach is used,

as for instance in [20], which is equivalent to consider that the scatterers are of infinite extent; it is thus important to better understand the influence of the height of the scatterers in the insertion loss of the system. For that purpose, three different scatterer heights are considered, namely 2m, 3m and 4m. In addition, the model presented in [20] is used to compute a purely 2D response, to be used as a reference. One should note that, by comparing these 2D results with the pure 3D results of the present paper, it becomes possible to assess the importance of the diffraction effect occurring at the top of the sonic crystal, a subject that has not been addressed yet in a systematic manner in the published literature, to the authors' best knowledge. Figure 13a presents the insertion loss curves calculated for the 4 cases now mentioned, in periodic configurations with 3 rows. Observing this figure, it is possible to see that the IL tends to increase progressively with the height of the sonic crystal, with differences of just 0.2 dB being registered between heights of 2m and 4m for the first band-gap frequency. When comparing to the reference result, it can be concluded that the 3D insertion loss also progressively approaches the 2D case, although it does not reach the same IL magnitude. Indeed, at 1000 Hz, a small difference of less than 1 dB is still registered between the case with taller scatterers and the 2D case; this difference rises to around 3 dB for the second band-gap, confirming that an overestimation of the insertion loss exists when 2D models are used, but also indicating that the diffraction effect is not as significant as in the case of classic noise barriers. It seems that, for the case of sonic crystals, the diffraction effect is not as pronounced as in a continuous wall; this was expected to occur since sonic crystals do not have a continuous and pronounced edge to produce such marked diffraction phenomenon. In Figure 13b an additional comparison is performed, now considering the hybrid model proposed in reference [13], for the case of scatterers 2.0m tall. That simplified approach just combines the IL provided by two 2D simulations, one considering the x-z plane, and another for the

x-y plane. For the tested case, a tendency for the simplified hybrid approach to overestimate the attenuation provided by the sonic crystal occurs throughout the whole spectrum, and it is particularly noticeable in the low frequency range and at the second band-gap. However, the position of the band-gaps is still correctly predicted by the simplified approach. In spite of this, it seems that the estimation obtained for this case is not as good as that computed using a pure 2D model, as seen in Figure 13a.

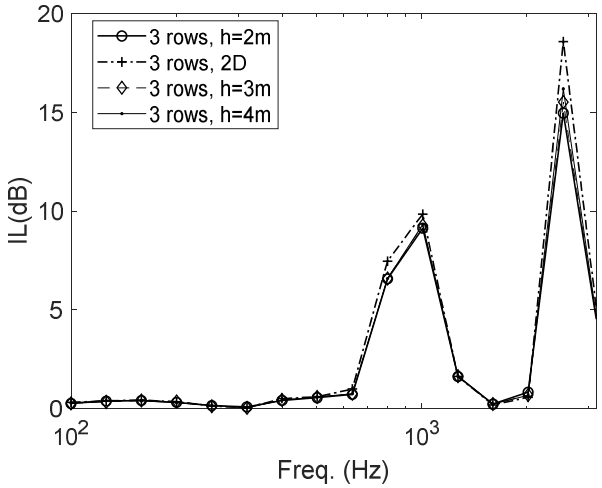

Figure 13 – Insertion loss in 1/3 octave bands of sonic crystals with 3 rows and a radius of 50% of the maximum: a) comparison between scatterers 2m, 3m and 4m tall, and a 2D analysis; b) comparison with the hybrid model of [13] for the case of h=2m.

To further analyze the diffraction effect occurring in the case of sonic crystals, different relative positions of the grid of receivers with respect to the barrier were evaluated, considering L=0.5 m, L=2.5 m, L=5.0 m and L=10.0 m (see Figure 9). One should note

that receivers placed further away from the barrier will typically be less protected from the incident wave field, and will receive a stronger contribution of diffracted energy by the top of the barrier. Therefore, observing Figure 14, where the IL curves for these four receiver positions are depicted, it becomes quite clear that the four curves are almost coincident up to the second band-gap, where some slight differences are registered. This coincidence further confirms that diffracted energy is not predominant in the case of sonic crystals, for which the dominant effect is the direct transmission of sound energy through the barrier itself.

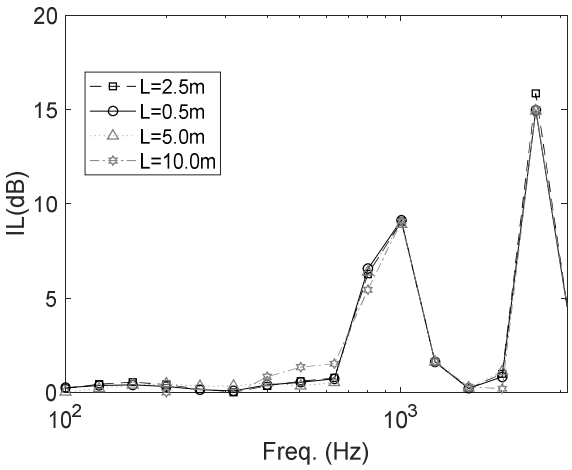

Figure 14 – Insertion loss in 1/3 octave bands computed for sonic crystals with scatterers 2m tall, for four different positions of the grid of receivers; 3 rows and a radius of 50% of the maximum value are considered.

6 Final remarks

In the present paper, the authors presented a new approach for the analysis of 3D acoustic problems with infinite periodicity along one direction, making use of the MFS. The proposed method has been developed in order to allow dealing with sonic crystals made of 3D scatterers, infinitely repeated with constant spacing along one direction, with efficiency. For that purpose, a specific periodic fundamental solution has been developed and studied, evidencing good convergence properties, and allowing problems with 3D

sonic crystals to be effectively handled using an elegant meshless method as the MFS. It should be pointed out that the proposed approach allows overcoming some significant drawbacks identified for the MFS, avoiding the full discretization of a large number of scatterers, thus reducing the problem size and computational costs. Comparison with a previously published model, also developed by the authors, indicates that this new model can accurately compute the response for infinite arrays with only a fraction of the computational cost. Parametric studies have been performed using the periodic MFS approach, and allowed reaching interesting conclusions. For example, it has been shown that the diffraction effect occurring at the top of the sonic crystal is not as evident as in the case of conventional (wall-type) noise barriers, and so the dominant phenomenon is the direct sound transmission of energy through the barrier with discrete periodic scatterers.

Acknowledgements

The authors acknowledge the financial support of FCT – Foundation for Science and Technology and COMPETE, through research project PTDC/ECM-COM/1364/2014. This work was partly financed by FEDER funds through the Competitivity Factors Operational Programme - COMPETE and by national funds through FCT – Foundation for Science and Technology within the scope of the project POCI-01-0145-FEDER-007633 and through the Regional Operational Programme CENTRO2020 within the scope of the project CENTRO-01-0145-FEDER-000006.

This work was also partially supported by the Spanish “Ministerio de Economia y Competitividad” under the project TEC2015-68076-R.

The EU funding support in the scope of COST (European Cooperation in Science and Technology) through the COST Action CA15125 – DENORMS: “Designs for Noise Reducing Materials and Structures” is here also acknowledged.

References

1. Martínez-Sala, R., Sancho, J., Sánchez, J. V., Gómez, V., Llinares, J., & Meseguer, F. (1995). Sound attenuation by sculpture. Nature, 378(6554), 241.
2. Sanchez-Perez, J. V., Rubio, C., Martinez-Sala, R., Sanchez-Grandia, R., & Gomez, V. (2002). Acoustic barriers based on periodic arrays of scatterers. Applied Physics Letters, 81(27), 5240-5242.
3. Umnova, O., Attenborough, K., & Linton, C. M. (2006). Effects of porous covering on sound attenuation by periodic arrays of cylinders. The Journal of the Acoustical Society of America, 119(1), 278-284.
4. Martínez-Sala, R., Rubio, C., García-Raffi, L. M., Sánchez-Pérez, J. V., Sánchez-Pérez, E. A., & Llinares, J. (2006). Control of noise by trees arranged like sonic crystals. Journal of Sound and Vibration, 291(1-2), 100-106.
5. Castiñeira-Ibáñez, S., Rubio, C., Romero-García, V., Sánchez-Pérez, J. V., & García-Raffi, L. M. (2012). Design, manufacture and characterization of an acoustic barrier made of multi-phenomena cylindrical scatterers arranged in a fractal-based geometry. Archives of Acoustics, 37(4), 455-462.
6. Kafesaki, M., & Economou, E. N. (1999). Multiple-scattering theory for three-dimensional periodic acoustic composites. Physical review B, 60(17), 11993.
7. Cao, Y., Hou, Z., & Liu, Y. (2004). Convergence problem of plane-wave expansion method for phononic crystals. Physics Letters A, 327(2-3), 247-253.
8. Yan, Z. Z., & Wang, Y. S. (2006). Wavelet-based method for calculating elastic band-gaps of two-dimensional phononic crystals. Physical review B, 74(22), 224303.
9. Cao, Y., Hou, Z., & Liu, Y. (2004). Finite difference time domain method for band-structure calculations of two-dimensional phononic crystals. Solid state communications, 132(8), 539-543.

10. Li, F. L., Wang, Y. S., Zhang, C., & Yu, G. L. (2013). Band-gap calculations of two-dimensional solid–fluid phononic crystals with the boundary element method. Wave Motion, 50(3), 525-541.

11. Koussa, F., Defrance, J., Jean, P., & Blanc-Benon, P. (2013). Acoustical efficiency of a sonic crystal assisted noise barrier. Acta acustica united with acustica, 99(3), 399-409.

12. Karimi, M., Croaker, P., & Kessissoglou, N. (2016). Boundary element solution for periodic acoustic problems. Journal of Sound and Vibration, 360, 129-139.

13. Castiñeira-Ibáñez, S., Rubio, C., & Sánchez-Pérez, J. V. (2013). Acoustic wave diffraction at the upper edge of a two-dimensional periodic array of finite rigid cylinders. A comprehensive design model of periodicity-based devices. EPL (Europhysics Letters), 101(6), 64002.

14. Zheng, H., Zhang, C., Wang, Y., Sladek, J., & Sladek, V. (2016). Band structure computation of in-plane elastic waves in 2D phononic crystals by a meshfree local RBF collocation method. Engineering Analysis with Boundary Elements, 66, 77-90.

15. Zheng, H., Zhang, C., Wang, Y., Sladek, J., & Sladek, V. (2016). A meshfree local RBF collocation method for anti-plane transverse elastic wave propagation analysis in 2D phononic crystals. Journal of Computational Physics, 305, 997-1014.

16. Yan, Z. Z., Wei, C. Q., Zheng, H., & Zhang, C. (2016). Phononic band structures and stability analysis using radial basis function method with consideration of different interface models. Physica B: Condensed Matter, 489, 1-11.

17. Kondapalli, P. S., Shippy, D. J., & Fairweather, G. (1992). Analysis of acoustic scattering in fluids and solids by the method of fundamental solutions. The Journal of the Acoustical Society of America, 91(4), 1844-1854.

18. Golberg, M. A., & Chen, C. S. (1998). The method of fundamental solutions for potential, Helmholtz and diffusion problems. Boundary integral methods-numerical and mathematical aspects, 103-176.

19. Godinho, L. M. C., Costa, E. G. A., Pereira, A. S. C., & Santiago, J. A. F. (2012). Some observations on the behavior of the method of fundamental solutions in 3d

acoustic problems. International Journal of Computational Methods, 9(04), 1250049.

20. Martins, M., Godinho, L., & Picado-Santos, L. (2013). Numerical evaluation of sound attenuation provided by periodic structures. Archives of Acoustics, 38(4), 503-516.

21. Santos, P. G., Carbajo, J., Godinho, L., & Ramis, J. (2014). Sound Propagation Analysis on Sonic Crystal Elastic Structures using the Method of Fundamental Solutions (MFS). Computers, Materials and Continua, 43(2), 109-136.

22. Godinho, L., Soares Jr, D., & Santos, P. G. (2016). Efficient analysis of sound propagation in sonic crystals using an ACA–MFS approach. Engineering Analysis with Boundary Elements, 69, 72-85.

23. Godinho, L., Amado-Mendes, P., Pereira, A., & Soares Jr, D. (2018). An Efficient MFS Formulation for the Analysis of Acoustic Scattering by Periodic Structures. Journal of Theoretical and Computational Acoustics, 26(01), 1850003.

24. Tadeu, A. J. B., & Godinho, L. M. C. (1999). Three-dimensional wave scattering by a fixed cylindrical inclusion submerged in a fluid medium. Engineering analysis with boundary elements, 23(9), 745-755.

25. Godinho, L., António, J., & Tadeu, A. (2001). 3D sound scattering by rigid barriers in the vicinity of tall buildings. Applied Acoustics, 62(11), 1229-1248.

26. Redondo, J., Picó, R., Roig, B., & Avis, M. R. (2007). Time domain simulation of sound diffusers using finite-difference schemes. Acta acustica united with acustica, 93(4), 611-622.